Nucleon-induced deuteron breakup: Analysis of 14.1 MeV data by rigorous Faddeev calculations with meson-exchange *NN* interactions

H. Witała,* W. Glöckle, and Th. Cornelius
Institut für Theoretische Physik II, Ruhr-Universität Bochum, D-4630 Bochum 1, West Germany
(Received 19 July 1988)

Kinematically complete breakup experiments for final-state interaction and collinear configurations have been analyzed by rigorous Faddeev calculations. The two-nucleon Paris potential and a one-boson-exchange parametrization of the new Bonn potential have been used. The treatment of charge-dependent forces in the Faddeev scheme is discussed and a simple $\frac{2}{3}$-$\frac{1}{3}$ rule is derived. In the collinear configuration a significant discrepancy is found between theoretical and experimental cross sections.

I. INTRODUCTION

Recently kinematically complete breakup experiments for the process ^{2}H$(p,pp)n$ at $E_p^{\rm lab}=14.1$ MeV have been performed.[1] The aim was to study selected kinematical configurations, final-state interaction (FSI) and collinear ones, which are possibly sensitive to three-nucleon force effects.[2] The data were analyzed by Faddeev calculations using phenomenological finite rank two-nucleon potentials and a perturbative inclusion of Coulomb effects. The fair agreement with the experimental data led to the conclusion that very little space is left for three-nucleon force effects. In the present work we analyze the data again by rigorous Faddeev calculations in the continuum using the Paris potential[3] and two one-boson-exchange parametrizations of the new Bonn potential [OBEPQ-version *A* (Ref. 4) and *B* (Ref. 5)]. Since the breakup cross sections in the FSI regions are very sensitive to $^1S_0$ *NN* forces we also take into account in this partial wave the difference between *nn* and *np* forces. No Coloumb effects will be included.

In Sec. II we briefly review our technique of solving modified Alt-Grassberger-Sandhas (AGS) equations and describe how we treat charge-dependent *NN* forces. Our results are presented and discussed in Sec. III. We summarize in Sec. IV.

II. THEORETICAL FORMULATION

We solve modified AGS equations[6]

$$T=tP+tPG_0T \tag{1}$$

as described in Ref. 7. That equation is more convenient for numerical work than the original AGS equations,[8] since the deuteron pole occurring in the $^3S_1$-$^3D_1$ partial wave state of the two-body *t*-operator t is not "smeared out" into logarithmic singularities by the action of the permutation operator P. If t acts on the pair 23 then $P=P_{12}P_{23}+P_{13}P_{23}$. The operator G_0 is the free three-particle propagator. Equation (1) is solved in momentum space and in a partial wave basis, which is truncated due to our assumption that the two-nucleon forces act only in the states with total two-body angular momentum $j\leq 2$. This leads to 34 angular momentum and isospin combinations for each conserved total angular momentum J and parity state [except for $J=\frac{3}{2}$ $(\frac{1}{2})$, where that number is 30 (18)]. The deuteron pole and the logarithmic "moving singularities" resulting from G_0 require special care as described in Ref. 7.

The operator T determines the transition operator for the breakup process

$$U_0=(1+P)T \ . \tag{2}$$

It is well established[9] that *np* and *nn* (or *pp*) forces are different in the state $^1S_0$. Also FSI maxima in the breakup cross section depend sensitively on force properties and especially on the two-nucleon scattering lengths in the state $^1S_0$. Therefore it is to be expected that neither the Paris potential, which is fitted to the *pp* data, nor the new Bonn potential, which is fitted to the *np* data, is fully adequate for a quantitative description of the FSI regions.

We take into account the charge dependence of the two-nucleon forces in the following way. We work in the frame work of the generalized Pauli principle. The two-nucleon *t*-operator for a system of two neutrons and one proton has the general form

$$t=P_{nn}t_{nn}P_{nn}+P_{np}t_{np}P_{np} \ , \tag{3}$$

where P_{nn} and P_{np} project on a neutron-neutron and a neutron-proton pair, respectively.

These projection operators can be written in terms of two-body isospin states as

$$P_{nn}=|t=1,t_z=1\rangle\langle t=1,t_z=1| \ , \tag{4}$$

$$P_{np}=\sum_{t=0,1}|t,t_z=0\rangle\langle t,t_z=0| \ . \tag{5}$$

If we neglect the very weak transition between $t=0$ and $t=1$ states in the *np* system, (3) reads

$$t=|t=1,t_z=1\rangle t_{nn}^{t=1}\langle t=1,t_z=1| +|t=1,t_z=0\rangle t_{np}^{t=0}\langle t=1,t_z=0| +|t=0,t_z=0\rangle t_{np}^{t=1}\langle t=0,t_z=0| \ . \quad (6)$$

Three isospin $\frac{1}{2}$ particles can form the three-particle states $|(t\frac{1}{2})T\rangle$ with total isospin $T=\frac{1}{2}$ or $\frac{3}{2}$ and subsystem isospins $t=0,1$. In that basis the two-nucleon t-operator (6) acting in the two-nucleon subsystem is easily shown to have the form

$$\langle(t\tfrac{1}{2})T|t|(t'\tfrac{1}{2})T'\rangle=\delta_{tt'}\delta_{TT'}\delta_{T\,1/2}[\delta_{t0}t_{np}^{t=0}+\delta_{t1}(\tfrac{2}{3}t_{nn}^{t=1}+\tfrac{1}{3}t_{np}^{t=1})] +\delta_{tt'}\bar{\delta}_{TT'}\frac{\sqrt{2}}{3}(t_{nn}^{t=1}-t_{np}^{t=1})+\delta_{tt'}\delta_{TT'}\delta_{T\,3/2}(\tfrac{2}{3}t_{np}^{t=1}+\tfrac{1}{3}t_{nn}^{t=1}) \ , \quad (7)$$

where $\bar{\delta}_{ij}=1-\delta_{ij}$.

In the first term on the right-hand side one can read off the prescription of choosing the t-operators in the state $T=\frac{1}{2}$. We refer to the special linear combination for $t=1$ as the $\frac{2}{3}$-$\frac{1}{3}$ rule for the t-operator. In the second term on the right-hand side we see that the transitions between $T=\frac{1}{2}$ and $T=\frac{3}{2}$ states are caused by the differences of nn and np forces. Finally the third term yields another $\frac{2}{3}$-$\frac{1}{3}$ rule within the state $T=\frac{3}{2}$. Note that for $T=\frac{3}{2}$ the roles of t_{np} and t_{nn} are interchanged in comparison to $T=\frac{1}{2}$.

Let us denote the three-body momentum-space partial wave basis including isospin by $|pq\alpha\rangle$ for $T=\frac{1}{2}$ and by $|pq\beta\rangle$ for $T=\frac{3}{2}$. Then apparently Eq. (1) decomposes into two coupled sets:

$$\begin{aligned}\langle pq\alpha|T|\phi\rangle&=\langle pq\alpha|t|p'q'\alpha'\rangle\langle p'q'\alpha'|P|\phi\rangle\\&\quad+\langle pq\alpha|t|p'q'\alpha'\rangle\langle p'q'\alpha'|PG_0T|\phi\rangle\\&\quad+\langle pq\alpha|t|p'q'\beta'\rangle\langle p'q'\beta'|PG_0T|\phi\rangle \ ,\\ \langle pq\beta|T|\phi\rangle&=\langle pq\beta|t|p'q'\alpha'\rangle\langle p'q'\alpha'P|\phi\rangle\\&\quad+\langle pq\beta|t|p'q'\alpha'\rangle\langle p'q'\alpha'|PG_0T|\phi\rangle\\&\quad+\langle pq\beta|t|p'q'\beta'\rangle\langle p'q'\beta'|PG_0T|\phi\rangle \ .\end{aligned} \quad (8)$$

In that shorthand notation integrations and summations are assumed in the primed quantities. Since the permutation operator P cannot change the total isospin, and the initial state $|\phi\rangle$ as a product of a deuteron and a free-nucleon wave function has isospin $T=\frac{1}{2}$, no matrix elements $\langle p'q'\beta'|P|\phi\rangle$ occur. The coupling between $|pq\alpha\rangle$ and $|pq\beta\rangle$ states is caused by the nonvanishing second term on the right-hand side in Eq. (7). That small effect is especially of interest for the state $^1S_0$. In this work we neglect the $T=\frac{3}{2}$ admixture altogether but keep the $\frac{2}{3}$-$\frac{1}{3}$ rule for the t-operator as prescribed in the first term on the right-hand side of Eq. (7).

III. RESULTS

The numerical performance has been carried through as basically described in Ref. 7 and with the same number of quadrature points as in Ref. 10. Let us denote the participating particles as:

$^2\mathrm{H}(n,n(1)n(2))p(3)$.

We first regard the FSI configuration. For the angular set up of the detectors for particles 1 and 2 ($\theta_1=52.6°$, $\theta_2=40.5°$, $\phi_{12}=180°$) two np FSI peaks occur along the kinematically allowed curve which is measured by the arc length S. The peak in Fig. 1 around $S\approx4$ MeV is caused by an interacting pn pair (13) produced at an angle of 52.6° and the peak at $S\approx13$ MeV by the other pair (23) produced at an angle of 40.5°. The curves are theoretical predictions where the two-nucleon forces are allowed to act only in the states $^1S_0$ and $^3S_1$-$^3D_1$. The solid curve is based on the Paris potential and is clearly too low in the peak heights. The dashed-dotted curve is a charge-dependent calculation according to the $\frac{2}{3}$-$\frac{1}{3}$ rule in the state $^1S_0$, where the np force is given by the OBEPQ (B) potential and the nn force by the Paris potential. In the states $^3S_1$-$^3D_1$ the Paris potential has been used. That $\frac{2}{3}$-$\frac{1}{3}$ rule effectively increases the $^1S_0$ scattering length from $a=-16.46$ fm for the Paris potential to $a=-18.89$ fm. The scattering length for both OBE parametrizations of the Bonn potential is $a=-23.76$ fm. The prediction for OBEPQ (B) is shown by the dashed

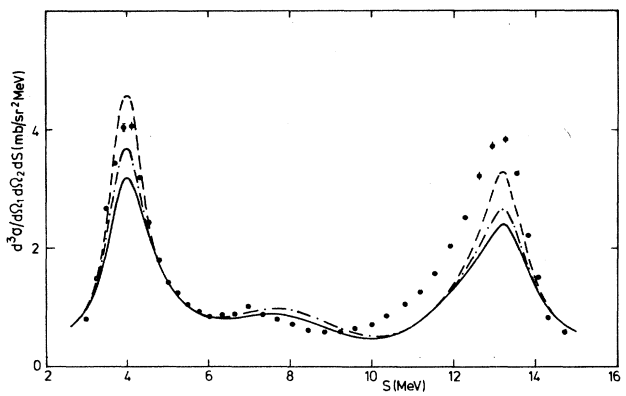

FIG. 1. Differential cross section as a function of the arc length S for the FSI situation with $\theta_1=52.6°$, $\phi_1=0°$, $\theta_2=40.5°$, and $\phi_2=180°$. Closed circles are experimental data taken from Ref. 1. Solid and dashed curves are predictions of the Paris and OBEPQ (B) potentials, respectively. The dashed-dotted curve is the result of a charge-dependent calculation with the "$\frac{2}{3}$-$\frac{1}{3}$" rule (see text). In these calculations two-nucleon interactions were restricted to act in $^1S_0$ and $^3S_1$-$^3D_1$ partial waves only.

curve in Fig. 1. With the larger scattering length the maximum in the FSI peaks increases as is well known, for instance, from a Migdal-Watson approximation.

In Fig. 2 the theoretical predictions are based on two-nucleon forces acting in all two-nucleon states with $j \leq 2$. Comparing the dashed-dotted curves in Figs. 1 and 2 belonging to the charge-dependent calculation one sees that the effect of the p- and d-wave two-nucleon forces is non-negligible. In this calculation the Paris potential is used for all partial waves except for the wave $^1S_0$, where the $\frac{2}{3}$-$\frac{1}{3}$ rule is applied as described above.

The same effect of p- and d-wave forces is seen for the Paris and OBEPQ potential predictions (compare Figs. 1 and 2). In the maxima of the cross section the effect of p and d waves is of the order of 12%. It should be noted that the version B (Ref. 5) has been introduced to improve the description of the mixing parameter ε_1 in the state $^3S_1$-$^3D_1$ (Ref. 10) over the older version A.[4] Clearly the charge-dependent calculation, which corresponds to our best dynamics presently at hand, deviates systematically from the data between the peaks and in the right one.

The experimental performance deviates from our ideal point geometry due to finite angular and energy resolutions. The experimental data in the figures are the result of a projection on the kinematical curve corresponding to point geometry.[1] In order to get a feeling for the variation of the breakup cross section caused by small angular changes we considered two additional angular pairs:

$$\theta_1 = 54.6°, \quad \theta_2 = 42.5°$$

and

$$\theta_1 = 54.6°, \quad \theta_2 = 38.5° \quad (\phi_{12} = 180°) .$$

The kinematically allowed curves for the three angular pairs are displayed for the two FSI regions in Fig. 3. As in Ref. 1 the arc lengths start ($S = 0$) from the point with minimum value E_1 and the larger of the possible two values of E_2 and run clockwise. These small angular variations cause a rather dramatic effect on the breakup

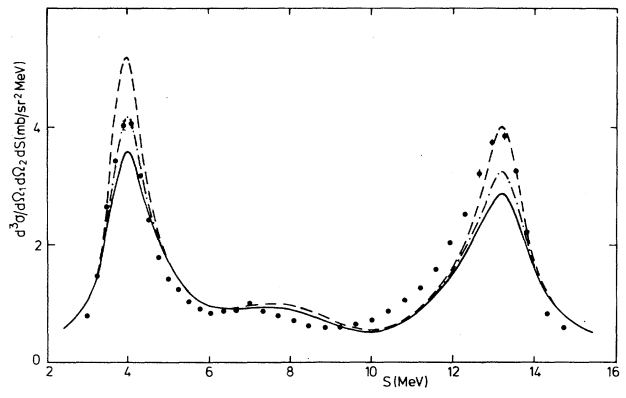

FIG. 2. See Fig. 1 for explanations. Now the dashed curve is the prediction of the OBEPQ (A) potential, and the two-nucleon forces act in all partial waves with $j \leq 2$.

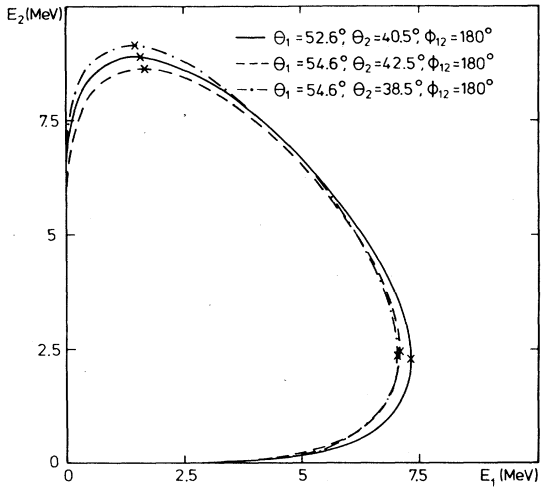

FIG. 3. Kinematical curves corresponding to different pairs of angles for particles 1 and 2 around the experimental point geometry (continuous curve) for a FSI situation. The crosses give the position of the maxima of the cross section on the corresponding curves (see Fig. 4).

cross section as shown in Fig. 4. This is especially true for the right FSI peak and for the cross section in the region between the peaks. All the curves in Fig. 4 are the results of a charge-dependent calculation.

In reality according to the experimental setup the θ uncertainties are smaller:[13] $\Delta\theta = \pm 0.53°$. Out of the four possibilities ($\pm\Delta\theta_1$, $\pm\Delta\theta_2$) we selected the two with the largest effects in increasing or decreasing the cross sections. These are $\theta_1 = 53.13°$, $\theta_2 = 41.03°$ and $\theta_1 = 53.13°$, $\theta_2 = 39.97°$. The resulting cross sections are shown in Fig. 5. The effects are now much smaller than in Fig. 4 and it is not possible to explain the discrepancy between theory and experiment in the right peak area by angular

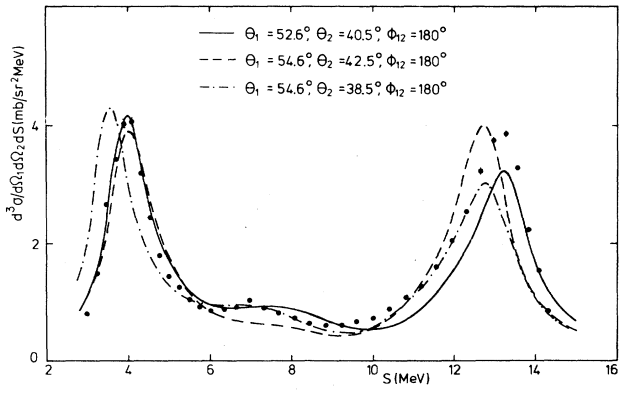

FIG. 4. Differential cross section as a function of the arc length S for the FSI situation and for different combinations of angles θ_1, θ_2 from Fig. 3. The calculations are charge-dependent and with two-nucleon forces acting in all $j \leq 2$ partial waves.

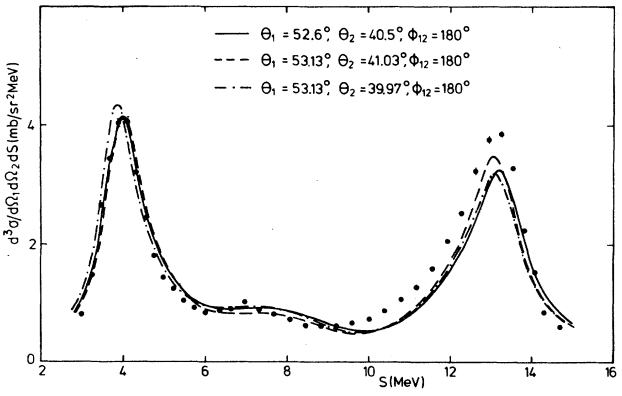

FIG. 5. The same as in Fig. 4 for three angular pairs demonstrating the sensitivity of the cross section to actual angular uncertainties (Ref. 13).

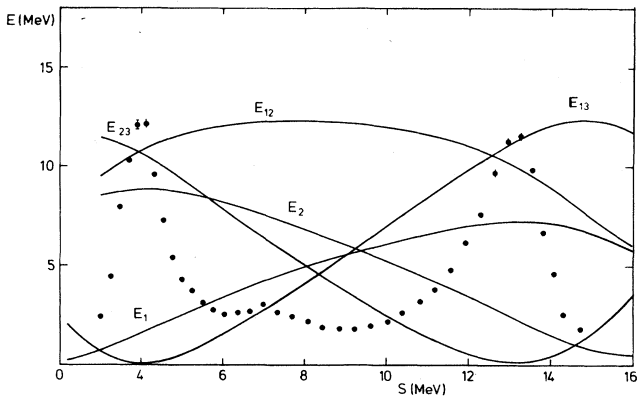

FIG. 6. Energies of different particles and relative energies for different pairs for the FSI situation and experimental point geometry as a function of the arc length S.

uncertainties $\Delta\theta$. The detector shapes were rectangular which led to an azimuthal uncertainty of $\Delta\phi = \pm 1.5°$. We calculated the cross section modifying $\phi_{12} = 180°$ by $\Delta\phi_{12} = 3°$ with essentially no effect (changes smaller than $\approx 3\%$). Energy uncertainties of the beam particles due to the finite thickness of the target are estimated[13] to be of the order of 100 keV. We calculated the breakup cross sections for $E = 14.0$ and 14.2 MeV using, however, the dynamical amplitudes determined for $E = 14.1$ MeV. The effects were extremely small ($< 2\%$). Also an exact calculation at $E = 13.0$ MeV and an interpolation to energies in the neighborhood of $E = 14.1$ MeV cannot explain the existing discrepancy in Fig. 2 in the peak maxima. Therefore we are forced to conclude that the meson-based two-nucleon forces we are using (including charge dependence) are unable to describe the measured breakup cross sections for all arc-length positions. While the left FSI peak is quite well reproduced we lie definitely below the data of the right peak and the theory shows a systematic shift in the region between the peaks in comparison to the data.

A last remark concerns possible Coulomb effects which are not taken into account in our calculation. We show in Fig. 6 various energies along the arc length S: the relative energy E_{23} which reaches zero in the right peak together with the energy E_1 of the "spectator" particle," the relative energy E_{13} which reaches zero in the left peak together with the energy E_2 of the "spectator particle," and finally the relative energy E_{12}. We see that the relative energy of the two neutrons (protons in the experiment), E_{12}, in and between the peaks is always of the order of 10 MeV or larger. Also the spectator energies E_1 and E_2 are always 6 MeV or larger in the peak areas. In view of the Coulomb barrier height for $p+d$ of about 200 keV one is tempted to assume that Coulomb effects are small under these kinematical conditions.

Let us now regard the collinear case, where the proton (neutron in the experiment) has zero c.m. energy and correspondingly the three nucleons are on a line in the c.m. system. We see from Fig. 7 that the detector angles θ_1 and θ_2 for the collinear case are close to the angular regions where the two np FSI conditions are fulfilled. Therefore the collinear configurations will be flanked by the slopes of two FSI peaks.

Again we start the presentation of our theoretical results with two-nucleon forces acting only in the states $^1S_0$ and $^3S_1$-$^3D_1$. In Fig. 8 the theoretical prediction for OBEPQ (B) is shown as a dashed curve, the one for the Paris potential as a continuous curve and the charge-dependent calculation as a dashed-dotted curve. All the curves lie too low in comparison to the experimental data. This changes if we include p- and d-wave forces as shown in Fig. 9. The prediction of the charge-dependent calculation (dashed-dotted curve), our "best dynamics" at

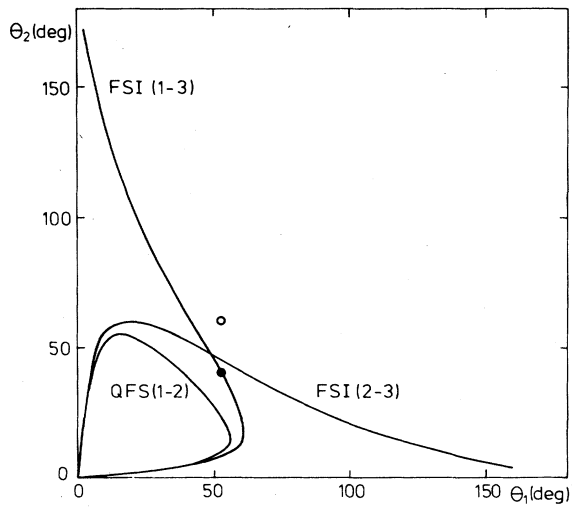

FIG. 7. θ_1-θ_2 locations of special kinematical configurations for $E_p = 14.1$ MeV. QFS(1-2) denotes the quasifree scattering of particles 1 and 2 (in laboratory frame $E_3 = 0$). The closed and open circles are the positions of the FSI and collinear situations, respectively, discussed in this paper.

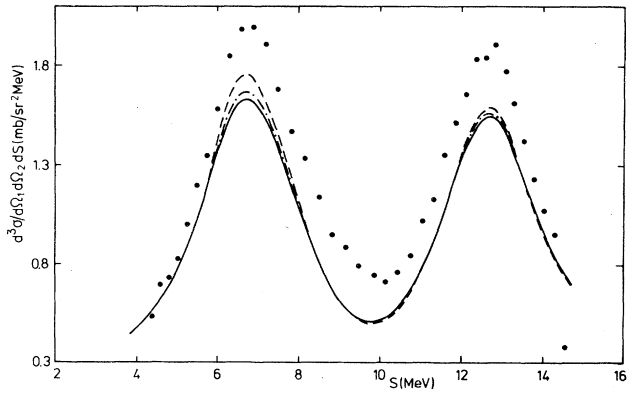

FIG. 8. Differential cross section as a function of the arc length S for the collinear situation with $\theta_1=52.6°$, $\phi_1=0°$, $\theta_2=60.5°$, $\phi_2=180°$ (the collinear region is at $S\approx 9.4$–10.2 MeV). Closed circles are experimental data taken from Ref. 1. For the explanation of the curves see Fig. 1.

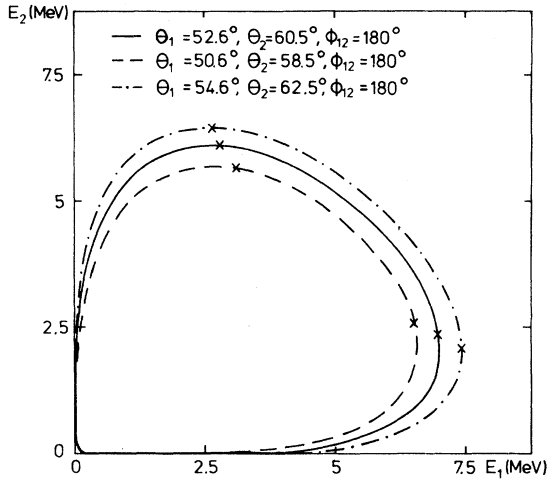

FIG. 10. Kinematical curves corresponding to different pairs of angles for particles 1 and 2 around the experimental point geometry (continuous curve) for the collinear situation. The crosses give the positions of the maxima of the cross section on the corresponding curves (see Fig. 11).

hand, lies below the data, especially in the collinear region between the peaks. It is important to realize that there the different curves in Figs. 8 and 9 coincide; in other words, the cross section in the collinear region is insensitive to modifications in the dynamical two-nucleon force input.

Let us now regard the sensitivity of the breakup cross section to variations in the angular positions of the detectors. In addition to the angular pair in the experiment, $\theta_1=52.6°$, $\theta_2=61.5°$, we also took $\theta_1=54.6°$, $\theta_2=62.5°$ and $\theta_1=50.6°$, $\theta_2=58.5°$. The corresponding three kinematical curves are shown in Fig. 10, the resulting breakup cross sections for charge-dependent calculations in Fig. 11. Again there are very dramatic changes in the maxima, similar to those discussed previously and shown in Fig. 4. The real angular uncertainties are, however, smaller, $\Delta\theta=\pm 0.53°$. We show in Fig. 12 the cross sections for the point geometry and for two angle variations thereof: $\theta_1=53.13°$, $\theta_2=61.03°$ and $\theta_1=52.07°$, $\theta_2=59.97°$. The effects are now much smaller and it is conceivable that a proper inspection of the raw data (before the projection on the kinematical curve for point geometry) could lead to an agreement with theory in the peak areas. The situation, however, is definitely different in the collinear region. There at $S\approx 9$–10.5 MeV it is not possible to fill the gap between theoretical predictions

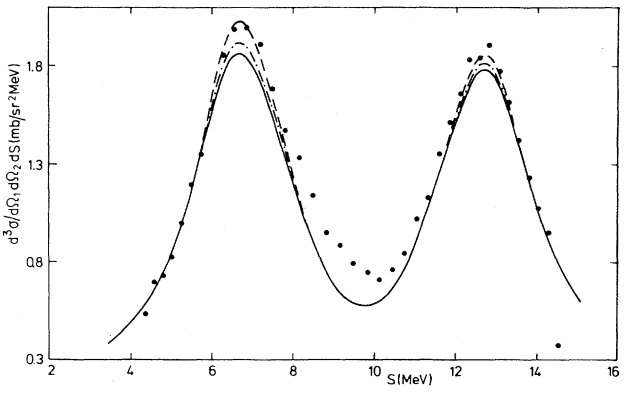

FIG. 9. See Fig. 8 for explanations. Here the dashed curve is the prediction of OBEPQ (A) potential and the two-nucleon forces act in all partial waves with $j\leq 2$.

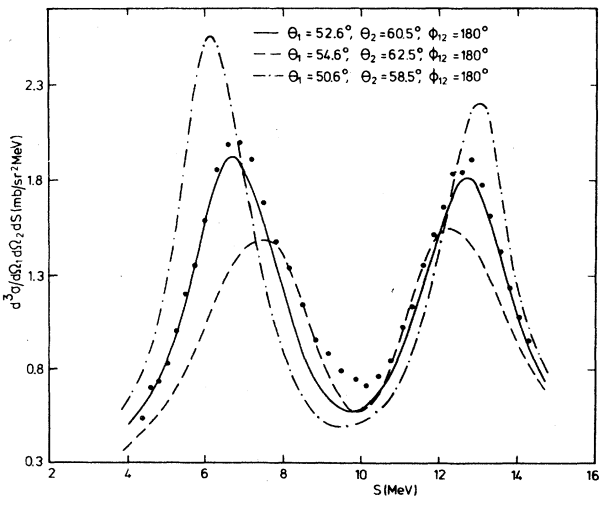

FIG. 11. Differential cross section as a function of the arc length S for the collinear situation and for different combinations of angles θ_1, θ_2 from Fig. 10. The calculations are charge dependent and two-nucleon forces act in all $j\leq 2$ partial waves.

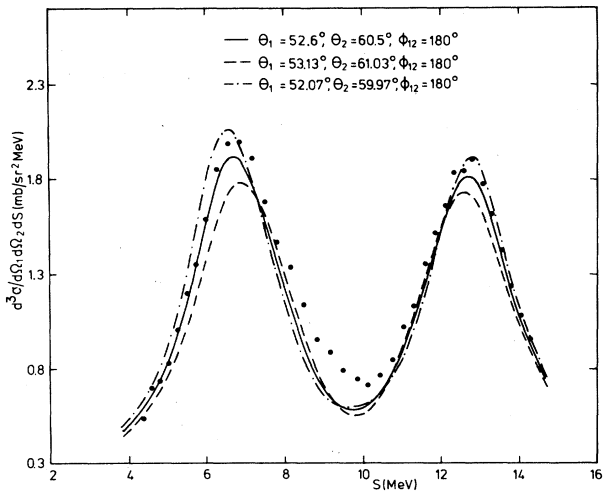

FIG. 12. The same as in Fig. 11 for three angular pairs demonstrating the sensitivity of the cross section to actual angular uncertainties.

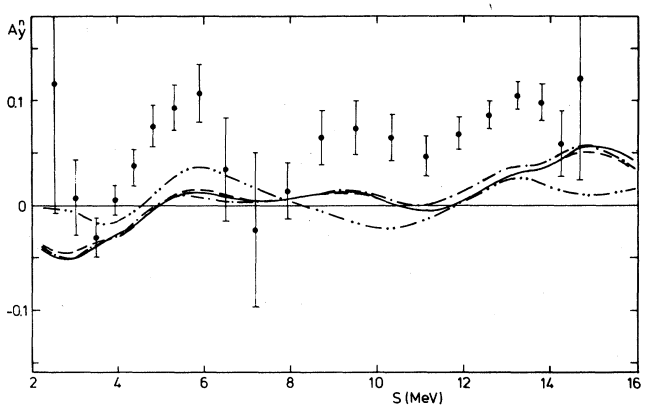

FIG. 14. The neutron analyzing power A_y^n as a function of the arc length S for the FSI situation and experimental point geometry. The closed circles are experimental data taken from Ref. 1. The continuous and dashed curves are predictions of the Paris and OBEPQ (A) potentials, respectively. The dashed-dotted curve is the result of the charge-dependent calculation with two-nucleon forces acting in all partial waves with $j \leq 2$. The dashed–double-dotted curve is a charge-dependent calculation with interactions acting in $^1S_0$ and $^3S_1$-$^3D_1$ partial waves only.

and the experimental data by variations of the angles. Moreover in this region the various energies, where neutrons (protons in the experiment) are involved, are not at all small, as seen in Fig. 13, therefore Coulomb effects are possibly small. We conclude that the discrepancy between theory and experimental data in the collinear region could be significant and possibly a signature of a three-nucleon force effect.

Let us finally regard in Figs. 14 and 15 analyzing powers in the FSI and collinear cases, respectively. The dashed–double-dotted curves refer to pure $^1S_0$ and $^3S_1$-$^3D_1$ forces and the charge-dependent calculation. Inclusion of p- and d-wave forces (all two nucleon states with $j \leq 2$) has a noticeable effect and leads to the three curves in Figs. 14 and 15, which essentially coincide. The three curves belong to the Paris (solid) potential, the OBEPQ (A) (dashed) potential, and to the charge-dependent calculation (dashed-dotted curve), respectively.

Especially for the FSI case there is a big discrepancy between the theoretical prediction and the experimental data. A similar study as for the cross section shows that changes in analyzing powers caused by taking the positions of both detectors different from the experimental point geometry cannot explain this discrepancy.

Also, energy variations of ± 100 keV for beam-particle energy have no significant effect. We refrain, however, from a definite conclusion because of the strong spread of the experimental data.

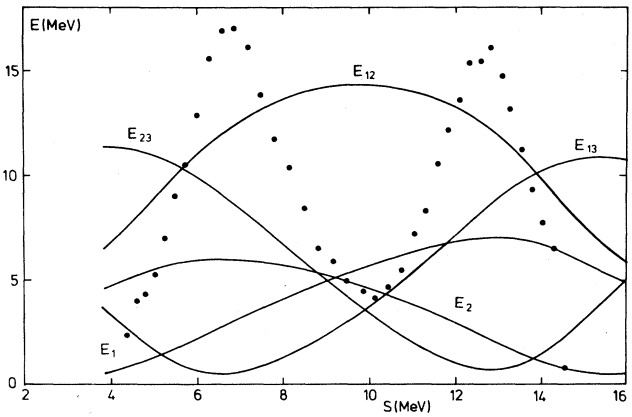

FIG. 13. Energies of different particles and relative energies for different pairs for the collinear situation and experimental point geometry as a function of the arc length S.

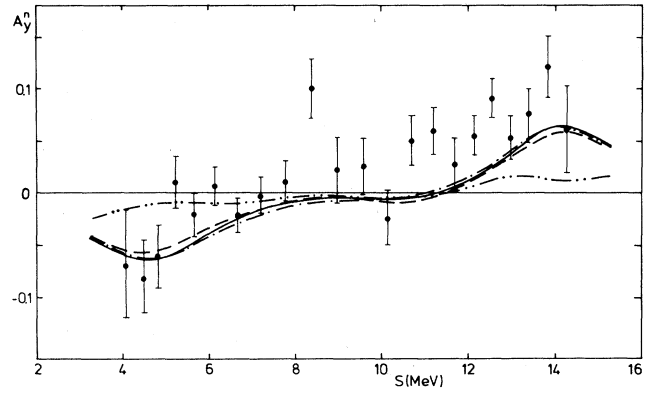

FIG. 15. The neutron analyzing power A_y^n as a function of the arc length S for the collinear situation and experimental point geometry. The closed circles are experimental data taken from Ref. 1. For explanation of curves see Fig. 14.

IV. SUMMARY

We analyzed recent experimental *pd*-breakup data in FSI and collinear configurations by rigorous Faddeev calculations using the Paris potential and two OBE parametrizations of the new Bonn potential. We also derived a rule of how to incorporate charge-dependent forces in the Faddeev scheme. Neglecting a $T=\frac{3}{2}$ admixture the simple recipe is, to use $t=\frac{2}{3}t_{np}+\frac{1}{3}t_{nn}$ as the two-nucleon t-operator for the $t=1$ states.

Calculations with the Paris potential and the OBE potential and taking into account a charge dependence of the two-nucleon force in the state $^1S_0$ were presented. The latter one turns out to be absolutely crucial for a useful analysis of FSI configurations. We have studied in FSI and collinear configurations the effect of varying the angles of the two detectors on the breakup cross section. For the angular uncertainties present in the experimental setup[13] of $\Delta\theta=\pm 0.53°$ these effects are not negligible. In projecting the experimental data onto the kinematical curve for point geometry these dynamical effects enter and lead to an "experimental cross section" along that ideal kinematical curve, which may deviate more or less from the true cross section along that curve. In a proper comparison with theory the theoretical cross-section data should be processed in the same manner as the experimental one. It is not done in this work. This could explain the small discrepancies between our charge-dependent calculation and the data in the two peaks flanking the collinear region in Fig. 8. It cannot explain the discrepancy in one of the FSI peaks (the right one) and in the region between the FSI peaks in Fig. 2.

The collinear region ($S\approx 9-10.5$ MeV) turns out to be insensitive to the potentials used (Fig. 9) and relatively insensitive to the angular uncertainties. There we see a definite discrepancy between the data and our theoretical two-nucleon force predictions. This could be a signature for the action of a three-nucleon force.

The experimental proton analyzing powers in both configurations, FSI and collinear, have large error bars and scatter strongly. Especially in the FSI case there is a big discrepancy between theory and experimental data which cannot be explained by changing the positions of the detectors, as is possible to some extent in the case of the cross section. Nevertheless, we refrain from a definite conclusion before experimental data with smaller error bars will be available.

It will be important to analyze more breakup configurations by rigorous Faddeev calculations using realistic meson-based two-nucleon forces to pin down cases of significant discrepancies between theoretical predictions and experimental data. A recent comparison[11] of experimental *nd* breakup data for $E=13.0$ MeV in the space-star configuration with our theoretical calculations revealed a strong discrepancy. On the other hand, at 10.3 MeV our theoretical results agree with experimental data in the same space-star configuration.[12] A significant discrepancy exists for the neutron analyzing power in elastic *nd* scattering.[10]

It will be important to improve on the calculation presented in Ref. 2 and perform rigorous Faddeev calculations including a 2π-exchange three-nucleon force to see its effect and to explore whether such a force is capable of curing specific discrepancies while showing no effect in cases where two-nucleon forces alone are sufficient.

ACKNOWLEDGMENTS

This work has been supported financially by the Deutsche Forschungsgemeinschaft. The numerical work has been performed on the CRAY X-MP/48 of the "Höchstleistungsrechenzentrum" in Jülich.

*Permanent address: Institute of Physics, Jagellonian University, PL-30059 Cracow, Poland.

[1]M. Karas, M. Buballa, J. Helten, B. Laumann, R. Melzer, P. Niessen, H. Oswald, G. Rauprich, J. Schulte-Uebbing, and H. Paetz gen. Schieck, Phys. Rev. C **31**, 1112 (1985).

[2]W. Meier and W. Glöckle, Phys. Lett. **138B**, 329 (1984).

[3]M. Lacombe, B. Loiseau, J. M. Richard, R. Vingh Mau, J. Côté, P. Pirès, and R. de Tourreill, Phys. Rev. C **21**, 861 (1980).

[4]R. Machleidt, K. Holinde, and Ch. Elster, Phys. Rep. **149**, 1 (1987).

[5]R. Machleidt (private communication).

[6]R. T. Cahill and I. H. Sloan, Nucl. Phys. **A165**, 161 (1971); W. M. Kloet and J. A. Tjon, Ann. Phys. (N.Y.) **79**, 407 (1973); A. Bömelburg, W. Glöckle, and W. Meier, in *Few-Body Problems in Physics,* edited by B. Zeitnitz (Elsevier, Amsterdam, 1984), Vol. II, p. 483.

[7]H. Witała, T. Cornelius, and W. Glöckle, Few-Body Systems **3**, 123 (1988).

[8]E. O. Alt, P. Grassberger, and W. Sandhas, Nucl. Phys. **B2**, 167 (1967).

[9]I. Ŝlaus, in *Few-Body Methods: Principles and Applications,* edited by T. K. Lim, C. G. Bao, D. P. Hou, and H. S. Huber (World Scientific, Singapore, 1986), p. 691.

[10]H. Witała, W. Glöckle, and T. Cornelius, Nucl. Phys. A (to be published).

[11]J. Strate, W. Geibdörfer, R. Lin, J. Cub, E. Finckh, K.Gebhardt, S. Schindler, H. Witała, W. Glöckle, and T. Cornelius, J. Phys. G (to be published).

[12]M. Stephan, K. Bodek, J. Krug, W. Lübcke, S. Obermanns, H. Rühl, M. Steinke, D. Kamke, H. Witała, T. Cornelius, and W. Glöckle, Phys. Rev. C (to be published).

[13]H. Paetz gen. Schiek (private communication).